SOFT/HARD FOCALIZATION IN THE EEG INVERSE PROBLEM

Teodor Iulian Alecu[1], Pascal Missonnier[2,3], Sviatoslav Voloshynovskiy[1], Pandelis Giannakopoulos[2,4] and Thierry Pun[1]

[1]Computer Vision and Multimedia Laboratory, University of Geneva, 24 Rue Général-Dufour, 1204 Geneva, Switzerland .phone: + (41) 22 379 1084, fax: + (41) 22 379 7780, email: Teodor.Alecu@cui.unige.ch.
[2]Neuroimaging Unit, [3]Service of Geriatric Psychiatry, Department of Psychiatry, University Hospitals of Geneva, 1225 Geneva, Switzerland.
[4]Service of Old Age Psychiatry, University Hospitals of Lausanne, 1008 Prilly, Switzerland.

ABSTRACT

We present in this paper a novel statistical based focalized reconstruction method for the underdetermined EEG (electroencephalogram) inverse problem. The algorithm is based on the representation of non-Gaussian distributions as an Infinite Mixture of Gaussians (IMG) and relies on an iterative procedure consisting out of alternated variance estimation/ linear inversion operations. By taking into account noise statistics, it performs implicit spurious data rejection and produces robust focalized solutions allowing for straightforward discrimination of active/non-active brain regions. We apply the proposed reconstruction procedure to average evoked potentials EEG data and compare the reconstruction results with the corresponding known physiological responses.

Keywords: EEG inverse problem, statistical regularization, Gaussian mixture, focalization

1. INTRODUCTION

Solving the EEG inverse problem arises in various medical fields as a tool for correct and relevant interpretation of EEG data. The goal is to map back the data measured on the scalp surface to the brain volume, allowing for direct physiological analysis. More recently, the EEG Inverse Problem has also emerged as a feature extraction tool in Brain-Computer Interface paradigms, aiming at classification procedures based on spatial discrimination of mental states.

In the search for the solution to the EEG Inverse Problem, two main directions have been pursued in the literature: dipole localization and distributed source model inversion.

The first type of algorithms search for the best fitting dipole for a given EEG data through (usually) non-linear optimization techniques. Multiple dipoles can be obtained either by a recursive search [3], or by initial decomposition of the EEG data using methods like PCA or ICA [2]. This type of procedures yield focalized solutions, but usually fail if correlated activity emerges in different parts of the brain.

Distributed source models perform reconstruction of the brain activity in the full brain volume, by formulating the EEG Inverse Problem as a linear inverse problem (see Section 2). However, the results given by the state-of-the art solutions are usually very smooth with respect to dipole localization methods, making it harder to discern between active/non-active regions.

We concentrate in this paper on a statistical based noise-robust focalization method for distributed source models in the EEG Inverse Problem. The rest of the paper is organized as follows: Section 2 briefly presents state-of-the art methods and introduces our reconstruction framework, Section 3 describes the statistical source model proposed, Section 4 defines the soft and soft/hard focalization algorithms and Section 5 presents a practical implementation and reconstruction results obtained with real EEG recordings.

2. RECONSTRUCTION FRAMEWORK

2.1 Linear formulation

The EEG inverse problem can be most generally formulated as a Fredholm integral equation of the first kind [1], while the most widely spread brain activity source model is that of a current dipole [1]. The discretization of the grey matter volume into volume pixels, usually denoted as *voxels*, allows the expression of the source-measurement relationship in classical linear vector-matrix form (**x**, **y** and **z** are column vectors):

$$\mathbf{y} = \mathbf{H}\mathbf{x} + \mathbf{z} \,, \qquad (1)$$

where **y** stands for the EEG measurements, **x** for the dipoles' amplitudes, and **H** is the lead-field matrix, containing on each column the measurements corresponding to unitary sources placed at the voxels' positions. We denote by N the number of electrodes and by M the number of voxels. Within a dipole model, to each voxel correspond three lead-field matrix columns, one for each orthogonal orientation in space along the cartesian axes, thus the size of the matrix **H** equals N by $3M$. The additive term **z** is added in order to account for measurement noise (electrode noise, power line interference etc.).

As a consequence of the nature of the EEG measurements, the problem (1) is underdetermined (the number of electrodes is usually much smaller than the number of voxels), and ill-posed in the Hadamard sense [7], requiring regularization.

2.2 Regularization

Existing state-of-the-art EEG inversion procedures [4], [5], [6] rely on deterministic regularization procedures based on minimization of quadratic functionals of the form:

$$\hat{\mathbf{x}} = \arg\min_{\mathbf{x}} \left(\left\| \mathbf{y} - \mathbf{H}\mathbf{x} \right\|^2 + \lambda \mathbf{x}^t \mathbf{W} \mathbf{x} \right), \qquad (2)$$

where the first term accounts for the discrepancy between the data and the reconstruction, and the second term is a minimum source energy condition. **W** can be a diagonal matrix (if one tackles energy minimization), a derivative filter (aiming at spatial source continuity) etc., and is sometimes weighted by the norm of the columns of the lead-field matrix, in order to insure deep brain sources reconstruction. Minimization of (2) in the underdetermined case leads directly to the linear solution:

$$\hat{\mathbf{x}} = \mathbf{W}^{-1}\mathbf{H}^t \left(\mathbf{H}\mathbf{W}^{-1}\mathbf{H}^t + \lambda \mathbf{I} \right)^{-1} \mathbf{y} \,. \qquad (3)$$

The Focuss procedure [6] iterates on the estimated solution and updates the weights of **W** with the energy of the previously estimated data, in a search for more focalized solutions. The main drawback of the Focuss procedure is its noise sensitivity caused by the trust it puts in the data.

We prefer to take a different point of view over the problem and reformulate it in a probabilistic framework. Thus, we treat **X**, **Y** and **Z** as random vector variables described by the corresponding distribution probabilities $p_{\mathbf{X}}(\mathbf{x})$, $p_{\mathbf{Y}}(\mathbf{y})$, $p_{\mathbf{Z}}(\mathbf{z})$, and we base our estimation on the *Maximum a Posteriori* (MAP) principle:

$$\hat{\mathbf{x}} = \arg\max_{\mathbf{x}} p_{\mathbf{X}|\mathbf{Y}} \left(\mathbf{x} \,|\, \mathbf{y} \right), \qquad (4)$$

which for independent variables can be rewritten as:

$$\hat{\mathbf{x}} = \arg\max_{\mathbf{x}} \left(p_{\mathbf{X}}(\mathbf{x})\, p_{\mathbf{Y}|\mathbf{X}} \left(\mathbf{y} \,|\, \mathbf{x} \right) \right). \qquad (5)$$

If the source and noise variables are zero-mean Gaussian distributed variables with covariance matrices $\mathbf{C}_{\mathbf{X}}$ and $\mathbf{C}_{\mathbf{z}}$:

$$\begin{aligned} p_{\mathbf{Z}}(\mathbf{z}) &= \frac{1}{\sqrt{(2\pi)^N \det(\mathbf{C}_{\mathbf{Z}})}} e^{-\frac{1}{2}\mathbf{z}^t \mathbf{C}_{\mathbf{Z}}^{-1} \mathbf{z}} \\ p_{\mathbf{X}}(\mathbf{x}) &= \frac{1}{\sqrt{(2\pi)^{3M} \det(\mathbf{C}_{\mathbf{X}})}} e^{-\frac{1}{2}\mathbf{x}^t \mathbf{C}_{\mathbf{X}}^{-1} \mathbf{x}}, \end{aligned} \qquad (6)$$

then by taking the log of (5) and inverting the sign, one eventually ends up with a regularization functional equivalent to (2), if $\mathbf{C}_{\mathbf{X}} = \mathbf{W}^{-1}$ and $\mathbf{C}_{\mathbf{z}} = \lambda \mathbf{I}$:

$$\hat{\mathbf{x}} = \arg\min_{\mathbf{x}} \left((\mathbf{y} - \mathbf{H}\mathbf{x})^t \mathbf{C}_{\mathbf{Z}}^{-1} (\mathbf{y} - \mathbf{H}\mathbf{x}) + \mathbf{x}^t \mathbf{C}_{\mathbf{X}}^{-1} \mathbf{x} \right), \qquad (7)$$

and with a linear solution given by:

$$\hat{\mathbf{x}} = \mathbf{C}_{\mathbf{X}} \mathbf{H}^t \left(\mathbf{H}\mathbf{C}_{\mathbf{X}}\mathbf{H}^t + \mathbf{C}_{\mathbf{Z}} \right)^{-1} \mathbf{y} \,. \qquad (8)$$

Unfortunately, if one of the involved probabilities is not Gaussian, the functional from (7) is no longer quadratic and the problem becomes non-linear. While keeping the assumption on noise Gaussianity, we tackle in the next sections the problem of MAP estimation of non-Gaussian source data through iterative linear regularization.

3. STATISTICAL SOURCE MODELING

We begin by assuming that the scalar variables $X[\mathrm{k}]$ of the vector **X** are independent identically distributed according to the scalar non-Gaussian probability distribution $p_X(x)$. We assume that this distribution is a zero-mean symmetric distribution, and that its Gaussian Transform $\mathcal{G}\left(p_X(x)\right)$ exists [8]. We recall that the Gaussian Transform $\mathcal{G}$ describes a symmetric distribution as an infinite mixture of Gaussians, and that the mixing function $G_X\left(\sigma^2\right) = \mathcal{G}\left(p_X(x)\right)$ satisfies:

$$\int_0^\infty G_X\left(\sigma^2\right) \mathcal{N}\left(x \,|\, \sigma^2\right) d\sigma^2 = p_X(x), \qquad (9)$$

where $\mathcal{N}\left(x \,|\, \sigma^2\right)$ is the zero-mean Gaussian distribution:

$$\mathcal{N}\left(x \,|\, \sigma^2\right) = \frac{1}{\sqrt{2\pi\sigma^2}} \mathrm{e}^{-x^2/2\sigma^2}.$$

Under these conditions we perform source splitting [9] and assume that the data is locally Gaussian, meaning that each local variable $X[\mathrm{k}]$ can be described as a zero-mean Gaussian variable with variance $\sigma_X^2[\mathrm{k}]$, and that the variances $\sigma_X^2[\mathrm{k}]$ are distributed accordingly to the distribution probability G_X. This amounts to a doubly stochastic representation of the data as:

$$\begin{aligned} & X[\mathrm{k}] \sim \mathcal{N}\left(x \,|\, \sigma_X^2[\mathrm{k}]\right);\ \sigma_X^2[\mathrm{k}] \sim G_X\left(\sigma^2\right) \\ & \mathbf{X} \sim \mathcal{N}\left(\mathbf{x} \,|\, \mathbf{C}_{\mathbf{X}}\right);\ \mathbf{C}_{\mathbf{X}} = \begin{pmatrix} \sigma_X^2[1] & & 0 \\ & \ddots & \\ 0 & & \sigma_X^2[3M] \end{pmatrix}. \end{aligned} \qquad (10)$$

4. SOFT FOCALIZATION ALGORITHM

Using the source modeling (10), one can use the linear solution (8), provided the variances $\sigma_X^2[\mathrm{k}]$ are known. Consequently, a supplementary step of variance estimation needs to be performed prior to data estimation. We propose therefore an iterative algorithm, which we call the soft focalization algorithm, denoted from now on as SF-IMG. It is constituted out of an initialization step and an estimation loop, as described below.

SF-IMG
Initialization: estimate $\mathbf{C}_{\mathbf{z}}$ and roughly estimate $\mathbf{C}_{\mathbf{X}}$.
Estimation loop :
  Estimate $\hat{\mathbf{x}}$ using (8);
  Convergence/error check (see 4.2);
    Exit or
    Estimate $\mathbf{C}_{\mathbf{X}}$ (see 4.1) and loop.

4.1 Variance estimation

In the context of the SF-IMG algorithm, we use a local MAP procedure for variance estimation, relying on the previous $\hat{x}[\mathrm{k}]$ estimate and on the Gaussian Transform G_X:

$$\hat{\sigma}_X^2[\mathrm{k}] = \arg\max_{\sigma_X^2[\mathrm{k}]} \left[G_X\left(\sigma_X^2[\mathrm{k}]\right) p\left(\hat{x}[\mathrm{k}] \,|\, \sigma_X^2[\mathrm{k}]\right) \right]. \qquad (11)$$

Since we assume additive Gaussian noise, the probability $p\left(\hat{x}[\mathrm{k}] \,|\, \sigma_X^2[\mathrm{k}]\right)$ can also be modelled as Gaussian. From (8):

$$\hat{\mathbf{x}} = \mathbf{G}\mathbf{H}\mathbf{x}_0 + \mathbf{G}\mathbf{z}\,, \tag{12}$$

where $\mathbf{G} = \mathbf{C}_\mathbf{X}\mathbf{H}^t\left(\mathbf{H}\mathbf{C}_\mathbf{X}\mathbf{H}^t + \mathbf{C}_\mathbf{Z}\right)^{-1}$ (8) and $\mathbf{x}_0$ denotes the original data. Under the assumption of independent data, the diagonal values of the covariance matrix $\mathbf{C}_{\hat{\mathbf{X}}}$ of the estimated data should be equal to:

$$\mathbf{C}_{\hat{\mathbf{X}}}[\mathrm{k},\mathrm{k}] = \sigma_X^2[\mathrm{k}]\left(\left(\mathbf{G}\mathbf{H}\right)^t\mathbf{G}\mathbf{H}\right)[\mathrm{k},\mathrm{k}] + \left(\mathbf{G}\mathbf{C}_\mathbf{Z}\mathbf{G}^t\right)[\mathrm{k},\mathrm{k}]\,. \tag{13}$$

If one does not take into consideration the non-diagonal elements of $\mathbf{C}_{\hat{\mathbf{X}}}$, the estimated data can be described locally as Gaussian (10), (12), with variance $\mathbf{C}_{\hat{\mathbf{X}}}[\mathrm{k},\mathrm{k}]$:

$$p\left(\hat{x}[\mathrm{k}] \mid \sigma_X^2[\mathrm{k}]\right) \sim \mathcal{N}\left(x \mid \mathbf{C}_{\hat{\mathbf{X}}}[\mathrm{k},\mathrm{k}]\right). \tag{14}$$

We exemplify the variance estimation procedure by setting p_X to be the Laplacian distribution (the Laplacian distribution is a particular member of the Generalized Gaussian family, whose Gaussian Transforms are detailed in [8]:

$$p_X\left(x \mid \lambda\right) = \frac{\lambda}{2}e^{-\lambda x}\,. \tag{15}$$

Its Gaussian Transform is given by [8], [9]:

$$G_X\left(\sigma^2\right) = \frac{\lambda^2}{2}e^{-\frac{\lambda^2}{2}\sigma^2}\,. \tag{16}$$

Considering that the estimation takes place within a neighbourhood of cardinality *m*, the result of (11) is:

$$\hat{\sigma}_X^2[k] = \max\left(\frac{1}{\beta}\left(\frac{2\sum\left\|\hat{x}\right\|^2}{m + \sqrt{m^2 + 4\lambda^2 \Big/ \beta\sum\left\|\hat{x}\right\|^2}} - \sigma_Z^2\right), 0\right), \tag{17}$$

where $\beta = \left(\left(\mathbf{G}\mathbf{H}\right)^t\mathbf{G}\mathbf{H}\right)[\mathrm{k},\mathrm{k}]$, and the sum is taken over all the samples in the selected neighbourhood.

4.2 Soft/Hard focalization

From (17) one can observe that some of the estimated variances might equal zero. The corresponding voxels will then naturally be dropped, amounting to a hard focalization procedure. In practice this criterion can be relaxed and one can drop all the voxels with an estimated variance smaller than a certain threshold relative to the maximum estimated variance (e.g. 5%). This relaxation allows for faster focalization and yields clearly defined active/non-active regions. We denote the resulting algorithm as ShF-IMG (soft/hard focalization).

The soft/hard focalization can be intuitively understood as a procedure which drops all sources who are covered by noise (17), acting as a spurious (noise induced) data rejection tool.

Accordingly, the iteration is said to have converged when no more voxels are dropped. The iterative procedure is also stopped if the energy of the projected error on the electrodes is bigger than the estimated noise variance:

$$\left\|\mathbf{y} - \mathbf{H}\hat{\mathbf{x}}\right\|^2 > \alpha Tr\left(\mathbf{C}_\mathbf{Z}\right), \tag{18}$$

where α is a constant (e.g. 2) setting up a confidence interval, and *Tr* indicates the trace of a matrix. The error check is imposed in order to stop possible divergence induced by inaccurate voxel drops.

5. IMPLEMENTATION AND RESULTS

We tested the ShF-IMG algorithm on real EEG averaged evoked potential data resulting from an odd-ball paradigm, i.e. detection of infrequent stimuli (patches with letters) among the standards stimuli (background patches without letters). The data was recorded using a symmetrical ear referenced 21 electrodes system at 1024 Hz, filtered with a zero phase-shift digital filter and a bandpass of 1 to 30 Hz (slope 24dB/octave), and averaged over 30 trials/subject for a total of 12 subjects and 360 trials. One artefacted electrode was dropped after visual examination.

We used for the reconstruction procedure a 4-layer homogeneous spherical head model of unitary radius as described in [10] and a voxel size of 0.06 (roughly 6mm), whereas the solution space was restrained to the grey matter, yielding a total of 4811 voxels. The lead-field matrix was computed according to the analytical expansion presented in [10].

5.1 Implementation

We begin by estimating the noise covariance matrix as the covariance of the EEG baseline, constituted out of the 200 ms before the trigger (odd-ball apparition)

$$\mathbf{C}_\mathbf{Z} = \mathrm{cov}\left(\mathbf{y}\left(t < trigger\right)\right). \tag{19}$$

We assume p_X to be Laplacian, which allows us to employ the analytical result (17) for variance estimation.

We perform then spatiotemporal inversion using a sliding window of length 5. For each window we start with the initialization of the ShF-IMG algorithm using a very rough approximation of $\mathbf{C}_\mathbf{X}$ as a diagonal matrix:

$$\mathbf{C}_\mathbf{X} = \frac{Tr\left(\mathrm{cov}\left(\mathbf{y}_\mathbf{w}\right) - \mathbf{C}_\mathbf{Z}\right)}{Tr\left(\mathbf{H}\mathbf{H}^t\right)}\mathbf{I}_{3M}\,, \tag{20}$$

where $\mathbf{y}_\mathbf{w}$ is a *N* by *T* matrix corresponding to the data in the current window. We enter then the estimation loop by performing (8). At each step the variance of the Laplacian distribution is re-evaluated as the mean variance of the estimated data:

$$\lambda^2 \Big/ 2 = \left\|\hat{\mathbf{x}}\right\|^2 \Big/ 3M\,, \tag{21}$$

and the local variances are calculated according to (17) using the temporal neighbourhood of the data (cardinality $m = T = 5$). Following the steps of ShF-IMG, we apply in succession the error check (18), the soft/hard focalization and the convergence check as defined in 4.2.

5.2 Reconstruction results

The perception of visual letters is known to elicit very specific evoked potentials responses [11], [12] over the scalp, such as the N75, P100, N120, N155, P200 and the later N2-N3 complex specifically modulated from attention to deviant stimuli (oddball paradigm). We present below the expected activated areas and the results of the reconstructions.

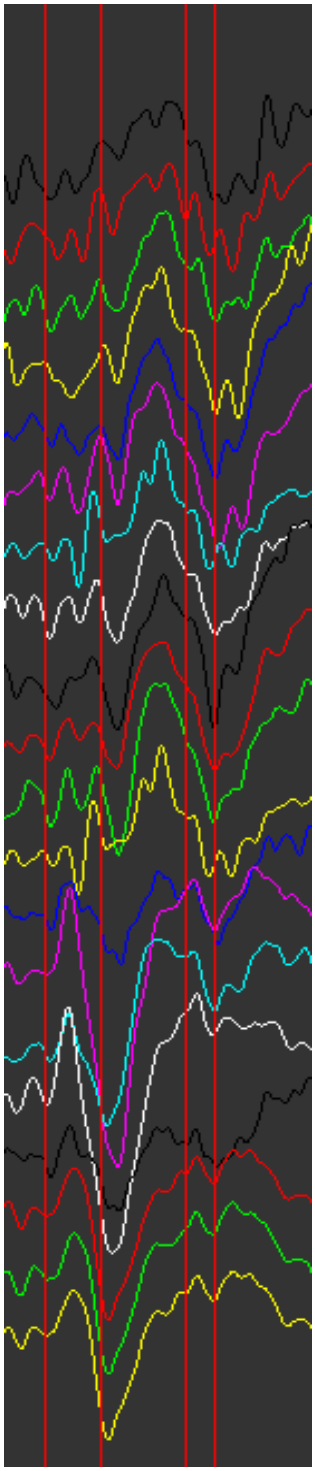

a. EEG recordings, the red vertical lines are positioned respectively at 75, 155, 280 and 320 ms

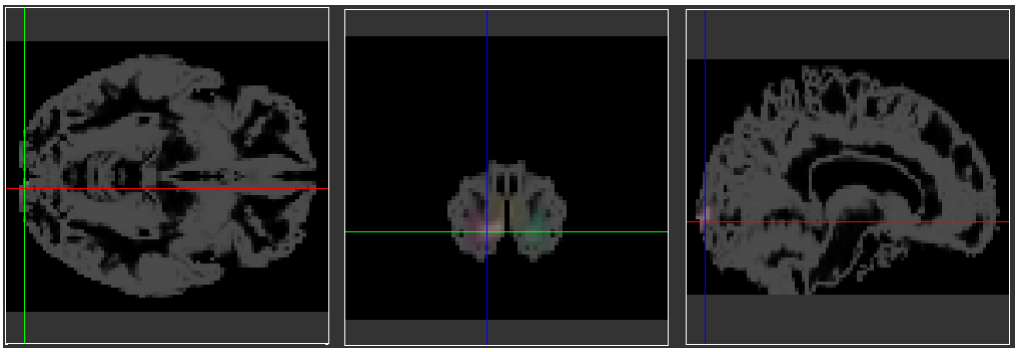

b N75 occipital response at 75 ms

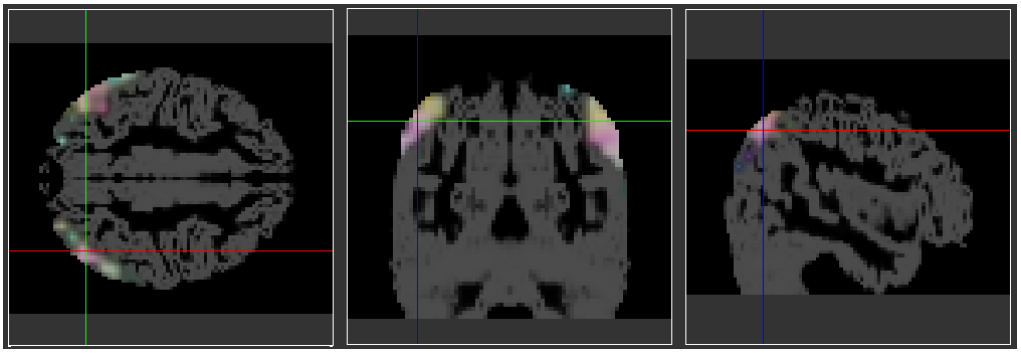

c N155 symmetric parietal response at 155 ms

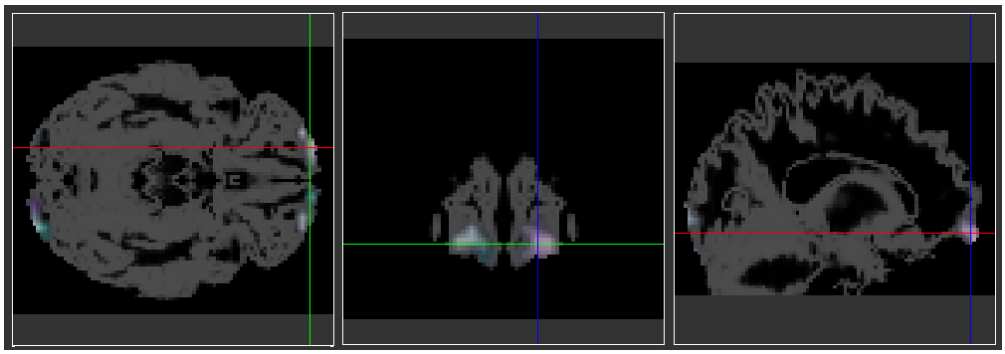

d. P300a frontal peak at 280 ms

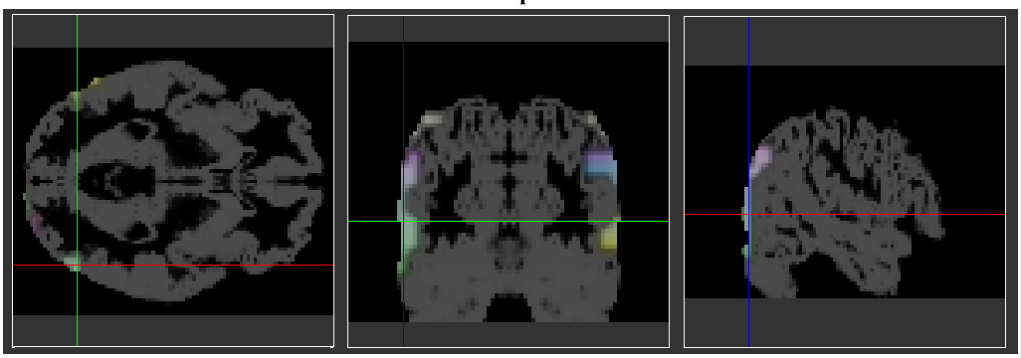

e. P300b parieto-temporal peak at 320 ms

Figure 1. Examples of reconstructions. EEG potential recordings to the left (a), reconstructions to the right (b-e)

N75: its origin is known to be in the occipital area. The reconstruction found a principal activity in the occipital area (see Fig. 1b).
P100 recorded over occipital sites: the origin is known to be occipital area and the generators activity diffuse on adjacent areas. The reconstruction identified activations in the occipital and parietal areas.
N120 recorded over fronto-central sites: expected multiple sources, a prefrontal generator was confirmed using implanted electrodes. The reconstruction identified activations in multiple areas, including frontal lobes.
N155 recorded over parietal sites: a symmetrical activity is expected in the parietal lobes. The reconstruction procedure identified a strong symmetrical activation of the parietal lobes and some secondary sources in the frontal lobes (see Fig. 1c).
P200 recorded over frontal, central and parietal sites: expected parietal and frontal activities. The reconstruction identified a principal parietal activation and a secondary frontal activation.
P300-P3a maximally recorded over frontal and central sites: distributed activation expected, principally in the prefrontal areas, cingulate gyrus, and posterior hippocampus. The reconstruction identified prefrontal, parietal and occipital activations.
P300-P3b maximally recorded over central and parietal sites following the P3a: principal activation expected in the parieto-temporal junction, prefrontal zones and the cingulate gyrus. The reconstruction identified activations in the parieto-temporal zones, central and prefrontal areas.
Although the P3a and P3b components of the P300 complex peak at different moments, they superpose in time. The P3a is characterized by a maximum anterior intensity, whereas the P3b presents a maximal posterior intensity. Our results show a maximum prefrontal activity at around 285 ms, corresponding with the expected P3a peak (see Fig. 1d), and a maximum parietal activity at around 320 ms, corresponding to the expected P3b peak (see Fig. 1e).
It can be observed that the reconstruction results are very close to the expected activations, but usually present supplementary sources with respect to the clinically confirmed active areas. This phenomenon might be caused by the low number of electrodes, impeding on the spatial resolution of the reconstruction, and by a possible noise overestimation which finally lead to oversmooth initial solutions not allowing proper focalization.

6. CONCLUSION

We presented in this paper a statistical framework and focalization procedure for the EEG Inverse Problem. We tackled in the same time the problem of regularization with non-Gaussian priors by introducing an iterative algorithm based on the Infinite Gaussian Mixture model and exemplified it with the Laplacian distribution. By properly using the noise statistics we introduced and justified the soft/hard focalization procedures, simultaneously performing spurious data rejection. The application of the proposed ShF-IMG reconstruction procedures showed that even with a low number of electrodes the algorithm is able to correctly identify simultaneously activated regions while rejecting most of the noise induced artefacts.
Still open questions remain, such as the identification of the source prior model, which we intend to model as a Generalized Gaussian distribution. In addition, a standardized procedure is needed to determine the noise statistics when one does not dispose of a baseline, e.g. single-trial recordings.

ACKNOWLEDGMENT

This work is supported by the Swiss NCCR (National Centre of Research) IM2 (Interactive Multimodal Information Management, http://www.im2.ch), the EU Network of Excellence Similar (http://www.similar.cc), and the Swiss National Foundation for Scientific Research, grant 3100-59110.99.

REFERENCES

1. J.C. Mosher, R.M Leahy, and P.S Lewis, “EEG and MEG: forward solutions for inverse methods”, IEEE Trans Biomed Eng, 1999, vol 46, n. 3, pp.245-259.
2. L. Zhukov, D. Weinstein, C.R. Johnson. “Independent Component Analysis for EEG Source Localization in Realistic Head Models,” In Proceedings of the IEEE Engineering in Medicine and Biology Society 22nd Annual International Conference, Vol. 3, No. 19, pp. 87--96. 2000.
3. Mosher, J.C.; Leahy, R.M., "Recursive MUSIC: A framework for EEG and MEG source localization", IEEE Transactions on Biomedical Engineering, Volume: 45 11 ,1998 , 1342-1354.
4. R .D. Pascual-Marqui, C. M. Michel, and D. Lehmann, "Low resolution electromagnetic tomography: a new method to localize electrical activity in the brain", Int. J. Psychophysiol. 18, pp. 49–65, 1994.
5. R. Grave de Peralta-Menendez, S. L. Gonzalez-Andino, "Comparison of Algorithms for the Localization of Focal Sources: Evaluation with simulated data and analysis of experimental data". IJBEM vol. 4, number 1, 2002.
6. Gorodnitsky IF, George JS, Rao BD. "Neuromagnetic source imaging with FOCUSS: a recursive weighted minimum norm algorithm". EEG and Clinical Neurophysiol., p. 231-251, 1995.
7. M.Bertero, P.Boccacci, "Introduction to Inverse Problems in Imaging", IOP Publishing, Bristol, 1998.
8. T. I. Alecu, S. Voloshynovskiy and T. Pun, "The Gaussian Transform", EUSIPCO2005, 13th European Signal Processing Conference, September 2005.
9. A. Hjørungnes, J. M. Lervik, and T. A. Ramstad , “Entropy Coding of Composite Sources Modeled by Infinite Mixture Gaussian Distributions”, in Proc. 1996 IEEE Digital Signal Processing Workshop , Loen, Norway, September 1996.
10. Z. Zhang, “A fast method to compute surface potentials generated by dipoles within multilayer anisotropic spheres”, Phys. Med. Biol 40, pp. 335-349, 1995.
11. S. Miller and F. Wood. "Electrophysiological indicants of black-white discrimination performances for letter and non-letter patterns", Intern J Neuroscience 1995;80:299-316.
12. P. Missonnier, U. Leonards, G. Gold, J. Palix, V. Ibanez, P. Giannakopoulos, "A new electrophysiological index for working memory load in humans", Neuroreport. 2003 Aug 6;14(11):1451-5.